

Research Article

Analysis for Resolution of Bistatic SAR Configuration with Geosynchronous Transmitter and UAV Receiver

Yicheng Jiang and Zhuoqun Wang

Research Institute of Electronic Engineering Technology, Harbin Institute of Technology, Number 714, Harbin 150001, China

Correspondence should be addressed to Zhuoqun Wang; wentingwangzhuoqun@126.com

Received 31 October 2012; Accepted 4 January 2013

Academic Editor: Gui Gao

Copyright © 2013 Y. Jiang and Z. Wang. This is an open access article distributed under the Creative Commons Attribution License, which permits unrestricted use, distribution, and reproduction in any medium, provided the original work is properly cited.

Bistatic SAR with geosynchronous illuminator and unmanned aerial vehicle receiver (GEO-UAV BiSAR) has significant potential advantages in the field of continuous local observation under a dangerous environment within nearly 24 h. Due to the extreme platform velocity differences, the ellipse orbital movement of GEOSAR makes this BiSAR configuration not like the conventional spaceborne BiSAR. In this paper, based on the orbital kinetic characteristic of GEOSAR, we theoretically analyze the variations of bistatic configuration effect on common azimuth coverage and coherent accumulated time. In addition, two-dimension the resolution is deduced by geometrical configuration on the basis of gradient method. The simulations show that the appropriate selection of initial bistatic configuration can restrain from the appearance of the dead zone in common coverage. And the image results are obtained by frequency domain RD based on Method of Series Reversion (MSR). It is shown that GEO-UAV BiSAR has the high resolution ability.

1. Introduction

Spaceborne synthetic aperture radar (SAR) has been applied to the wide fields such as landform measurement, ocean observation, earthquake monitor, and digital elevation model (DEM) [1]. For decades, lots of low-orbit (LEO) satellite emitted have high-resolution capability. However, beam irradiation extent of LEO is limited in dozens of kilometers near the nadir, and the revisit time is much longer. To this aspect, geosynchronous SAR (GEOSAR) can overcome the shortcomings aforementioned [2–4].

Geosynchronous orbits have the unique characteristic that their orbital period is nearly 24 h. It makes GEOSAR suitable for the continuous imaging on the specific partial region within 24 h [5]. And the ground coverage provided by a GEOSAR can be nearly one third of the globe for a highly inclined orbit, and it can be as small as few hundred kilometers for a SAR placed in a slightly inclined orbit [6].

Nevertheless, it requires a larger antenna to overcome the energy attenuation of the ionosphere and stratosphere [7–9]. There exists difficulties to hardware realization. In addition, imaging accumulation time, which reaches a few

hours, makes the imaging quality quite easier to be affected by unstable factors in larger ground coverage. To solve these problems, the literature [10] derives a space-based radar surveillance concept employing geosynchronous illumination and bistatic reception on either unmanned aerial vehicles (UAVs) or LEO. Due to the wide beam coverage of GEOSAR, it is easy to realize distributed imaging configuration with illuminator GEOSAR and multiple receivers (aircraft, UAV, LEO, and MEO satellites). Not only the wide imaging area is achieved, but also the requirements for the transmitted power and antenna size are reduced [11, 12].

In particular, bistatic geometrical configuration of GEOSAR illuminator and UAVSAR receiver (GEO-UAV BiSAR) may realize local observation in a dangerous environment. However, since the orbital characteristics of GEOSAR, we need to control the attitude of UAVSAR in the ground station for high resolution. Hence, it is different from other configurations, for example, GEO illumination and LEO receiver; GEO illumination and airborne receiver.

A key factor in determining the performance of GEO-UAV BiSAR systems is the two-dimensional resolution, but performance analysis of BiSAR characterized for any

configuration is usually complex. The literature [13] describes comprehensive knowledge regarding the resolution of BiSAR with geostationary illuminator and UAV receiver, which can be obtained from the gradient method in terms of time delay and the Doppler shift [14, 15]. Yet, it does not consider the variation of geometrical configuration as a function of time effect on resolution. In this case, the geostationary orbit is just a special one of geosynchronous orbit, and it ignores orbital motion and earth rotation effect on GEOSAR velocity, when orbit inclination is not equal to zero.

Before the imaging study for GEO-UAV BiSAR, its two-dimensional spectrum is demanded to discuss. Currently, the traditional method has two kinds, Loffeld's bistatic formula (LBF) [16, 17] and Method of Series Reversion (MSR) [18, 19]. The former mainly applies the Taylor expansion on phase histories of transmitter and receiver individually. The latter considers a power series method to count the stationary point of bistatic phase histories, and its accuracy is scalable in a sense. To this end, MSR is more applicable to the imaging study of GEO-UAV BiSAR.

This paper is organized as follows. It begins with a description of GEOSAR ground track in local ground coordinate system. Section 3 discusses the relative movement of two platforms effect on common coverage and coherent accumulated time owing to the extreme platform velocity differences. In Section 4, the formulas of two-dimensional resolution are deduced from the geometrical relationship of GEOSAR and UAVSAR based on gradient method. In Section 5, we analyze GEO-UAV BiSAR configuration influences on range and azimuth resolution by simulations. And proper initial selecting configuration can avoid the appearance of dead zone in the swath. Then, the imaging results by frequency domain RD method based on MSR are presented and analyzed.

2. Analyses to Movement Model of GEOSAR

2.1. Movement Track of GEOSAR. Suppose that GEOSAR runs on the ellipse orbit and the earth is uniform sphere, orbital inclination is i , right ascension of ascending node is Ω_0 , and argument of perigee is W_0 . The satellite position equation can be expressed in earth fixed coordinate system:

$$\begin{bmatrix} X_s(t_0 + t_a) \\ Y_s(t_0 + t_a) \\ Z_s(t_0 + t_a) \end{bmatrix} = RW_B(t_0 + t_a) W_A W_C(t_0 + t_a), \quad (1)$$

where

$$W_A = \begin{bmatrix} \cos \Omega_0 & -\sin \Omega_0 & 0 \\ \sin \Omega_0 & \cos \Omega_0 & 0 \\ 0 & 0 & 1 \end{bmatrix} \begin{bmatrix} 1 & 0 & 0 \\ 0 & \cos i & -\sin i \\ 0 & \sin i & \cos i \end{bmatrix}$$

$$\times \begin{bmatrix} \cos W_0 & -\sin W_0 & 0 \\ \sin W_0 & \cos W_0 & 0 \\ 0 & 0 & 1 \end{bmatrix},$$

$$W_B(t_0 + t_a) = \begin{bmatrix} \cos(\omega_e \cdot (t_0 + t_a)) & \sin(\omega_e \cdot (t_0 + t_a)) & 0 \\ -\sin(\omega_e \cdot (t_0 + t_a)) & \cos(\omega_e \cdot (t_0 + t_a)) & 0 \\ 0 & 0 & 1 \end{bmatrix}$$

$$W_C(t_0 + t_a) = \begin{bmatrix} \cos f(t_0 + t_a) & -\sin f(t_0 + t_a) & 0 \\ \sin f(t_0 + t_a) & \cos f(t_0 + t_a) & 0 \\ 0 & 0 & 1 \end{bmatrix} \quad (2)$$

t_0 is the center time point of time range, ω_e is the earth rotation angular velocity and R is the geocenter distance of the satellite.

In the time range foregoing, the velocity of GEOSAR related to the earth is given by

$$\vec{V}_{sT_EF}(t_0 + t_a) = \sqrt{\frac{\mu}{a}} W_A(t_0 + t_a) W_B \begin{bmatrix} -\sin f(t_0 + t_a) \\ \cos f(t_0 + t_a) \\ 0 \end{bmatrix} \\ + \begin{bmatrix} \omega_e Y_s(t_0 + t_a) \\ -\omega_e X_s(t_0 + t_a) \\ 0 \end{bmatrix}, \quad (3)$$

where a is a semimajor axis, μ is a gravitation constant, R_e is the earth radius, and H_T is a GEOSAR distance of ground.

Thus, when $i = 0$, GEOSAR is the stationary state and GEO-UAV BiSAR images in the local area near the equator. With the increase of i , \vec{V}_{sT} goes up gradually, and the variation of latitude is $[-i, i]$ in "Figure 8" imaging area. For maximum irradiation of Chinese territory, we choose $i = 60^\circ$. Based on GEOSAR basic parameters (see Table 1), the ground track of GEOSAR ($i \neq 0$) is shown in Figure 1.

Due to higher altitude of GEOSAR [20], the rate \vec{V}_{sT} at which the spacecraft moves along its orbital path is unequal to the rate \vec{V}_{eT} at which the footprint of the antenna beam moves along the surface of the earth: $\vec{V}_{eT} = R_e \vec{V}_{sT} / (R_e + H_T)$.

2.2. GEOSAR Velocity in Local Ground Coordinate System. In general, GEOSAR is described in earth-fixed coordinate system as well as UAVSAR in local ground coordinate system. We will convert GEOSAR into the local ground coordinate system in which the original point O represents the intersection between the satellite line of sight and the ground, the Ox -axis corresponds with track direction of GEOSAR, the Oz -axis corresponds with the connection between satellite and subpoint, and the Oy -axis is determined according to the right-hand rule (see Figure 2).

GEOSAR runs around the earth within a periodical time, T_s . In T_s , the range (Oy -axis) and the azimuth (Ox -axis) acceleration of GEOSAR ground track is shown in Figure 3.

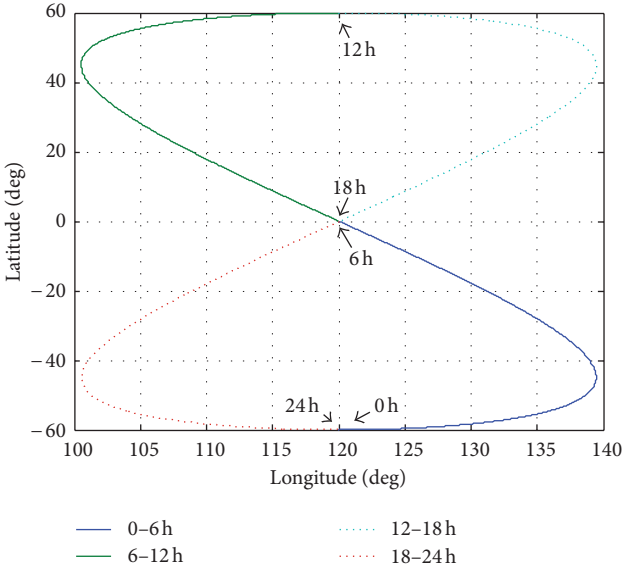


FIGURE 1: Ground track of 60° inclined geosynchronous orbit.

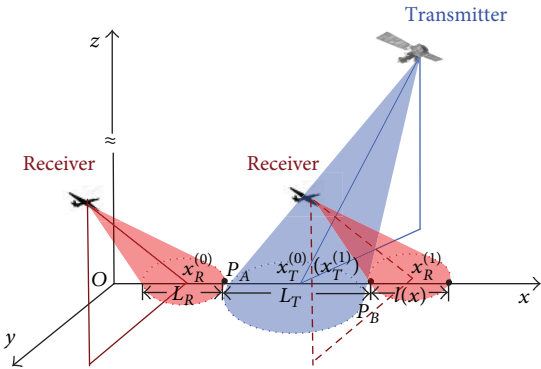


FIGURE 2: The GEOSAR and UAVSAR are in the local ground coordinate system, where the red region represents beam irradiation coverage of UAVSAR, and the blue is GEOSAR.

The trend of range acceleration is similar to a cosine curve whose period is $T_s/2$. The peak value is $2.236 \times 10^{-2} \text{ m/s}^2$, and the valley value is $3.9 \times 10^{-4} \text{ m/s}^2$. Furthermore, the trend of azimuth acceleration is similar to a sine curve whose period is $T_s/4$. The maximum is $9.0088 \times 10^{-3} \text{ m/s}^2$, and the minimum is $5.395 \times 10^{-4} \text{ m/s}^2$.

The range coverage of GEOSAR ground track $C_{tr} = R_{tc}\theta_{tran}/\sin(\theta_{tin}) = 3.75 \times 10^5 \text{ m}$ and the azimuth coverage $C_{ta} = R_{tc}\theta_{taim}/\cos(\varphi_{tsq}) = 1.25 \times 10^5 \text{ m}$ where θ_{tran} and θ_{taim} are the range and azimuth bandwidth of GEOSAR separately; θ_{tin} is an incidence angle, φ_{tsq} is a squint angle, when range acceleration a_a reaches peak, the surface coverage will deviate from the Ox-axis for $T_v > 4.0952 \times 10^3 \text{ s}$ (T_v represents common irradiation time, of two platforms; the limited time length T_{vlim} is calculated by the formula $C_{tr}/2 = \vec{V}_{eT} T_{vlim} + 1/2a_a T_{vlim}^2$). Besides, for the azimuth acceleration is much smaller, the ground track velocity of GEOSAR is considered

uniform motion as $\vec{V}_{eT}(t_0)$ in the condition of $T_v < 4.0952 \times 10^3 \text{ s}$.

3. Coherent Integration Time and Azimuth Common Coverage

Based on the theoretical research of resolution [21], the coherent integration time and azimuth common coverage influence azimuth resolution capability of GEO-UAV BiSAR.

Coherent integration time T_{sar} and azimuth coverage C_a are relative to GEOSAR azimuth coverage L_T , UAVSAR azimuth coverage L_R , and antenna footprint velocity of two platforms. Movement of GEOSAR is described as the uniform motion in T_v under the aforementioned study. While UAV is difficult to control motion stability in aerodynamic interference (roll angle, pitch angle, and heading angle of UAVSAR are variable). In this case, the accurate calculation is very troubling. To simplify calculation, we consider that roll angle, pitch angle and heading angle of UAVSAR are all constants, and UAV is a uniform motion in a straight line, \vec{V}_R . Therefore, the antenna footprint velocity ratio k can be shown as

$$k = \frac{\vec{e} \cdot \vec{V}_{eT}}{\vec{e} \cdot \vec{V}_R}, \quad (4)$$

where $\vec{e} = [1 \ 0 \ 0]^T$ is the azimuth unit vector.

- (1) If $k = 0$, GEOSAR is the stationary station.
- (2) If $k > 0$, UAV flies the same direction with transmitter. When $V_{eT} < V_R$, $k \in (0, 1)$, otherwise $k \in (1, +\infty)$.
- (3) If $k < 0$, UAV flies the opposite direction with transmitter.

Assume that footprint middle points of GEOSAR and UAVSAR are given by x_T and x_R , respectively, on the Ox-axis in Figure 2. Left and right edges of GEOSAR is P_A and P_B ; $P_A = [x_A \ 0 \ 0]^T$ and $P_B = [x_B \ 0 \ 0]^T$. If two platforms intersect at P_A , $x_T = x_T^{(0)}$ and $x_R = x_R^{(0)}$; if they intersect at P_B , $x_T = x_T^{(1)}$ and $x_R = x_R^{(1)}$. Then, $x_T^{(0)} = x_A + L_T/2$, $x_R^{(0)} = x_A - L_R/2$, $x_T^{(1)} = x_B - L_T/2$, and $x_R^{(1)} = x_B + L_R/2$.

For the subsequent simulation data show $V_{eT} > V_R$ (see Tables 1 and 2), we primarily discuss C_a and T_{sar} in the case of $k \in (1, +\infty)$. When $x_R = x_R^{(0)}$, $C_a = 0$, while $x_R = x_R^{(1)}$ and C_a achieve the maximum. Suppose that $l(x)$ represents the distance between the corresponding right edge points of the transmitter and the receiver in the Ox-axis. The change trend of $l(x)$ is $L_R \Rightarrow 0 \Rightarrow L_T$ with the relative movement of two platforms (see Figure 2). Thus, T_{sar} by (23) and (24) in the Appendix is calculated. Besides, the common irradiation time of two platforms is $T_v = C_a/V_R$.

Taking into account the difference value of k , we count C_a and T_{sar} , respectively (see the Appendix), when $k = 0$ and $C_a = L_T$. While in the case that V_{eT} , V_R , L_T , and L_R are constants, C_a is inversely proportional to $|V_{eT} - V_R|$ if

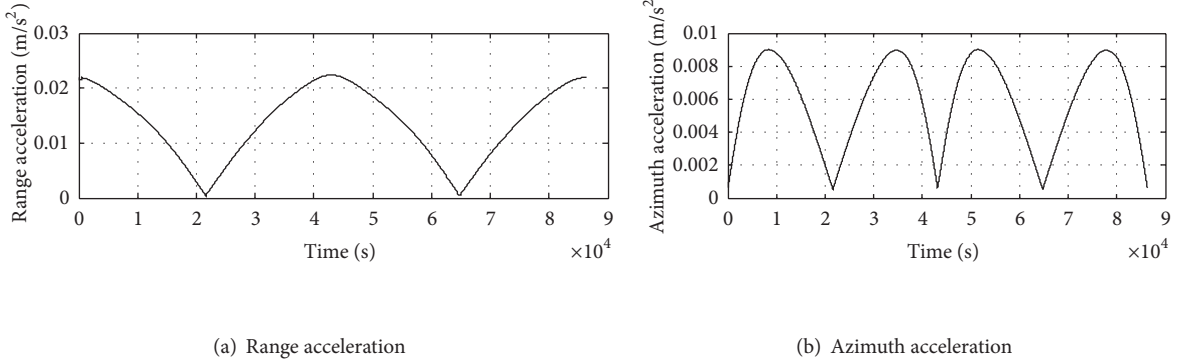


FIGURE 3: The range acceleration (a) and the azimuth acceleration (b) of GEOSAR ground track in local ground coordinate system.

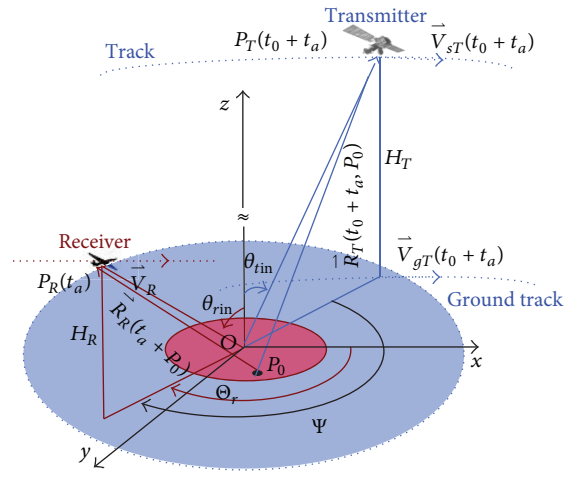


FIGURE 4: GEO-UAV BiSAR geometry.

TABLE 1: GEOSAR transmitter parameters.

GEOSAR parameters	Value
Orbit altitude	36000 km
Argument of perigee	90°
Right ascension of ascending node	30°
Orbit inclination	60°
Azimuth beam width	0.2°
Angle of elevation	0.6°

$k > 0$ ($|V_{eT} + V_R|$ if $k < 0$). And the maximum T_{sar} depends on the synthetic aperture time of receiver. If the coherent accumulated time is less than the maximum T_{sar} , the imaging quality is fuzzy in the zone which is known as “dead zone”. Conversely, it is called as “clear zone”.

4. Resolution of GEO-UAV BiSAR

GEO-UAV BiSAR geometry in local ground coordinate system is shown in Figure 4. The center of the scene is

TABLE 2: UAVSAR receiver parameters.

UAVSAR parameters	Value
Wavelength	0.03 m (X-band)
Bandwidth	150 MHz
Altitude	8 km
Incidence angle	1° ~80°
Angle between $R_T(t_0, O)$ and $R_R(t_0, O)$	0° ~360°
Antenna length	1 m

O point, GEOSAR locates $P_T(t_0 + t_a)$; UAVSAR locates $P_R(t_a)$. The time-domain matched filter is constructed by forming an instantaneous slant range to a point target $P_m = [x_m \ y_m \ z_m]^T$ referred to as the range equation

$$\overrightarrow{R}(t_s, P_s) \equiv \overrightarrow{R}_m(t_s + t_s, P_s) + \overrightarrow{R}_n(t_s, P_s), \quad (5)$$

where

$$\begin{aligned}\overrightarrow{R}_T(t_0 + t_a, P_m) &= P_T(t_0 + t_a) - P_m, \\ \overrightarrow{R}_R(t_a, P_m) &= P_R(t_a) - P_m = (P_R(0) - P_m) + \overrightarrow{V}_R t_a.\end{aligned}\quad (6)$$

Because GEOSAR shows a variable motion as $\vec{V}_{sT}(t_0 + t_a)$, the gradient of time delay $\vec{\nabla}t$ and the gradient of the Doppler shift $\vec{\nabla}f_a(t_a, P_m)$ are defined as (4.a) and (4.b):

$$\overrightarrow{\nabla t} = \frac{1}{c} \left(\frac{\overrightarrow{R}_T(t_0 + t_a, P_m)}{|\overrightarrow{R}_T(t_0 + t_a, P_m)|} + \frac{\overrightarrow{R}_R(t_a, P_m)}{|\overrightarrow{R}_R(t_a, P_m)|} \right). \quad (4.a)$$

Note that $\overrightarrow{\nabla f}_a(t_a, P_m)$ depends on the angular rate of two platforms. For $|\overrightarrow{V}_{sT}|/|\overrightarrow{R}_T(t_a, P_m)| = O(10^{-4})$ and $|\overrightarrow{V}_R|/|\overrightarrow{R}_R(t_a, P_m)| = (10^{-1})$, UAVSAR dominates $\overrightarrow{\nabla f}_a(t_a, P_m)$:

$$\begin{aligned} \overrightarrow{\nabla f}_a(t_a, P_m) &\approx \frac{1}{2\pi} \frac{\partial \nabla \Phi(t_a, P_m)}{\partial t_a} \\ &= -\frac{1}{\lambda} \left(\frac{1}{|\overrightarrow{R}_R(t_a, P_m)|} \left(\overrightarrow{V}_R - \left(\overrightarrow{V}_R \frac{\overrightarrow{R}_R(t_a, P_m)}{|\overrightarrow{R}_R(t_a, P_m)|} \right. \right. \right. \\ &\quad \times \left. \left. \left. \frac{\overrightarrow{R}_R(t_a, P_m)}{|\overrightarrow{R}_R(t_a, P_m)|} \right) \right), \end{aligned} \quad (7)$$

$$\begin{aligned} \overrightarrow{\nabla f}_a(t_a, P_m) &= \frac{1}{2\pi} \frac{\partial \nabla \Phi(t_a, P_m)}{\partial t_a} \\ &= -\frac{1}{2\pi} \times \frac{2\pi}{\lambda} \frac{\partial}{\partial t_a} \left(\frac{\overrightarrow{R}_T(t_0+t_a, P_m)}{|\overrightarrow{R}_T(t_0+t_a, P_m)|} + \frac{\overrightarrow{R}_R(t_a, P_m)}{|\overrightarrow{R}_R(t_a, P_m)|} \right) \\ &= -\frac{1}{\lambda} \left(\frac{1}{|\overrightarrow{R}_T(t_0+t_a, P_m)|} \right. \\ &\quad \times \left(\overrightarrow{V}_{sT}(t_0+t_a) \right. \\ &\quad \left. \left. - \left(\overrightarrow{V}_{sT}(t_0+t_a) \frac{\overrightarrow{R}_T(t_0+t_a, P_m)}{|\overrightarrow{R}_T(t_0+t_a, P_m)|} \right) \right. \\ &\quad \left. \times \frac{\overrightarrow{R}_T(t_0+t_a, P_m)}{|\overrightarrow{R}_T(t_0+t_a, P_m)|} \right) \\ &\quad + \frac{1}{|\overrightarrow{R}_R(t_a, P_m)|} \\ &\quad \times \left(\overrightarrow{V}_R - \left(\overrightarrow{V}_R \frac{\overrightarrow{R}_R(t_a, P_m)}{|\overrightarrow{R}_R(t_a, P_m)|} \right) \frac{\overrightarrow{R}_R(t_a, P_m)}{|\overrightarrow{R}_R(t_a, P_m)|} \right). \end{aligned} \quad (4.b)$$

The maximum delay time for movement in the ground plane is along the projection of $\overrightarrow{\nabla t}$ into xOy plane, $\overrightarrow{\nabla t}_e$. Similarly, the maximum change in the Doppler frequency moves along the projection of $\overrightarrow{\nabla f}_a$ into xOy plane, $\overrightarrow{\nabla f}_e$. Thus,

the range resolution D_r and the azimuth resolution D_a are given by

$$\begin{aligned} D_r &= \frac{1}{B_r |\overrightarrow{\nabla t}_e|} \cdot \frac{\overrightarrow{\nabla t}_e}{|\overrightarrow{\nabla t}_e|}, \\ D_a &= \frac{1}{|\overrightarrow{\nabla f}_e| T_{\text{sar}}} \cdot \frac{\overrightarrow{\nabla f}_e}{|\overrightarrow{\nabla f}_e|}. \end{aligned} \quad (8)$$

BiSAR resolution has the properties of time varying and spatial varying. On the basis of the GEO-UAV BiSAR geometry, (8) is redescribed as

$$\begin{aligned} D_r &= \frac{C}{2B_r \cos(\Psi/2)} \cdot \frac{\overrightarrow{\nabla t}_e}{|\overrightarrow{\nabla t}_e|}, \\ D_a &\approx \frac{H_R \lambda}{T_{\text{sar}} (t_0+t_a) V_R \cos \theta_{\text{rin}} \sqrt{1-\sin^2 \theta_{\text{rin}} \cos^2 (\Theta_r)}} \cdot \frac{\overrightarrow{\nabla f}_e}{|\overrightarrow{\nabla f}_e|}, \end{aligned} \quad (9)$$

where Ψ is the illuminator out-of-plane angle (with respect to the receiver and centered in the origin), Θ_r is the angle between the Ox -axis and the projection of UAVSAR position into xOy plane, and Θ_r is determined by Ψ .

The range resolution mainly depends on Ψ through (9). It attains the maximum for $\Psi = 180^\circ$ and the minimum values for $\Psi = 0^\circ$. In other words, the gradient of time delay has no component onto xOy plane for $\Psi = 180^\circ$, GEO-UAV BiSAR construction has the worst range resolution.

The azimuth resolution is relative to coherent accumulated time and the attitude change of UAV. With the shorter coherent accumulated time $T_{\text{sar}}(t_0 + t_a)$, the imaging quality of GEO-UAV BiSAR will decline gradually (dead zone1). Whereas, the azimuth resolution can further simplify as $D_a \approx D/\sqrt{1 - \sin^2 \theta_{\text{rin}} \cos^2 \Theta_r}$ in the clear zone. When θ_{rin} reaches an enough value, D_a is the maximum for $\Theta_r = 0^\circ, 180^\circ$, and 360° . And the gradient of the Doppler shift is the smallest component onto xOy plane.

For aforesaid reasons, the proper selection of original UAVSAR attitudes, θ_{rin} and Ψ , can make GEO-UAV BiSAR exhibit high resolution. To achieve this aim in clear zone, we will avoid the appearance of the worst construction in mutual movement process of transmitter and receiver. (Worst construction illuminates the area called dead zone2.)

In a periodical time of GEOSAR, the relative movement of GEOSAR and UAVSAR works in finite time $[t_0 - T_v/2, t_0 + T_v/2]$ (the local ground coordinate system is different for t_0 varying). Suppose that the original value of Ψ (corresponding t_0) is in CCI with regard to good imaging quality. For the sake of platform velocity differences, the variation range of Ψ , Ψ_{var} is still in CCI:

$$[\Psi - \max(\Psi_{\text{var}} - \Psi), \Psi + \max(\Psi_{\text{var}} - \Psi)] \in \text{CCI}, \quad (10)$$

where Ψ_{var} is related to the velocity ratio of the two platforms, k . Considering $k > 0$, Ψ_{var} is given by

$$\Psi_{\text{var}} = a \cos \left(\frac{\left(P_{s,\text{LS}}(t_0 + t_a) - \vec{V}_R \times t_a \right)}{\left| P_{s,\text{LS}}(t_0 + t_a) - \vec{V}_R \times t_a \right|} \cdot \frac{\vec{R}_R(t_a, P_m)}{\left| \vec{R}_R(t_a, P_m) \right|} \right), \quad (11)$$

where $P_{s,\text{LS}}(t_0 + t_a)$ is the GEOSAR subpoint. And (11) can be further simplified as

$$\Psi_{\text{var}} \approx a \cos \left(\frac{\left(P_{s,\text{LS}}(t_0) + \left| \vec{V}_{eT} - \vec{V}_R \right| \times t_a \right)}{\left| P_{s,\text{LS}}(t_0) + \left| \vec{V}_{eT} - \vec{V}_R \right| \times t_a \right|} \cdot \frac{\vec{R}_R(t_a, P_m)}{\left| \vec{R}_R(t_a, P_m) \right|} \right). \quad (12)$$

Since

$$\max(t_a) = \frac{T_v}{2} = \frac{V_R L_T - V_{eT} L_R}{2V_R \left| \vec{V}_{eT} - \vec{V}_R \right|}, \quad (13)$$

where $\max(\Psi_{\text{var}})$ is expressed as

$$\begin{aligned} \max(\Psi_{\text{var}}) \\ = a \cos \left(\frac{\left(P_{s,\text{LS}}(t_0) + \left(\vec{V}_R L_T - \vec{V}_{eT} L_R \right) / 2 \right)}{\left| P_{s,\text{LS}}(t_0) + \left(\vec{V}_R L_T - \vec{V}_{eT} L_R \right) / 2 \right|} \cdot \frac{\vec{R}_R(t_a, P_m)}{\left| \vec{R}_R(t_a, P_m) \right|} \right). \end{aligned} \quad (14)$$

To meet the condition of (10), $\max(\Psi_{\text{var}})$ will be in CCI also. Note from (14) that Ψ_{var} is related to \vec{V}_{eT} , L_R , \vec{V}_R , and L_T .

When $k < 0$, $\max(\Psi_{\text{var}})$ is the same to (14). However, GEOSAR runs on a circle orbit if $k = 0$. Under this circumstance, Ψ is meaningless for $\theta_{\text{rin}} = 0$. Hence, the range resolution is given by

$$D_r = \frac{C}{2B_r} \cdot \frac{\vec{V} t_e}{\left| \vec{V} t_e \right|}. \quad (15)$$

5. Simulation Analysis

In order to study the resolution of GEO-UAV BiSAR, we discuss the influence of coherent accumulated time and attitude change of UAV on the two-dimensional resolution. And the imaged results are disposed through using frequency domain RD method based on MSR.

5.1. Effect of Coherent Accumulated Time on Azimuth Resolution. Within a periodical time of GEOSAR, the velocity

TABLE 3: Azimuth coverage and coherent accumulated time of GEOSAR at different time instants.

Time t_0 (s)	$T_s/8$	$T_s/4$	$T_s/2$
V_{eT} (m/s)	366.54	464.15	232.08
Clear zone ($\times 10^4$ m)	[−2.09, 2.09]	[−1.49, 1.49]	[−3.95, 3.95]
Dead zone1 ($\times 10^4$ m)	[−2.12, 2.09] & [2.09, 2.12]	[−1.52, −1.49] & [1.49, 1.52]	[−3.98, −3.95] & [3.95, 3.98]
$\max(T_{\text{sar}})$ (s)	2.71	2.71	2.73

V_{eT} is a variable. The bistatic configuration changes with the different time instant t_0 selected (origin O is different with a function t_0 in local ground coordinate system). According to the parameters of GEOSAR and UAVSAR (see Tables 1 and 2), we can gain $k \in (1, +\infty)$. In the condition of $\theta_{\text{rin}} = 10^\circ$ and $\Psi = 311^\circ$, the azimuth coverage and the coherent accumulated time are calculated through (23) and (24) in the appendix. GEOSAR beam surface velocity, clear-zone, dead zone1, and coherent accumulated time for $t_0 = T_s/8$, $T_s/4$, and $T_s/2$ are shown in Table 3.

Simulations that demonstrate the azimuth coverage of GEO-UAV BiSAR are inversely proportional to $|V_{eT} - V_R|$. At a constant L_R , the size of dead zone1 shows a decrease with V_{eT} going up. The change of $\max(T_{\text{sar}})$ follows the squint angle of receiver that varies owing to the orbital movement of GEOSAR.

Taking $t_0 = T_s/8$ as an example, the influence of coherent accumulated time on azimuth resolution is drawn in Figure 5. In the clear zone, the azimuth resolution will achieve 0.99 m, while the azimuth resolution capability reduces with coherent accumulated time dropping gradually in the dead zone1.

5.2. Effect of the Initial Attitudes for Two Platforms on Resolution. Based on resolution analysis in Section 4, the appropriate attitude control of UAVSAR enables to avoid the appearance dead zone2 in the clear zone. As far as of range and the Doppler resolution are concerned, Figure 6 shows their variations as two functions of θ_{rin} and Ψ for GEO-UAV BiSAR ($t_0 = T_s/8$).

Ψ has a great effect on the range resolution, to which θ_{rin} is meaningless. If $\Psi \in [0^\circ, 90^\circ]$ and $\Psi \in [276^\circ, 360^\circ]$, BiSAR has higher resolution and $D_r \leq 1.4$ m. If $\Psi \in [91^\circ, 275^\circ]$, BiSAR resolution is much lower and $D_r > 1.4$ m. When $\Psi = 180^\circ$, it is the worst condition that gradient of time delay is equal to zero such that the range resolution reaches the maximum value (see Figure 6(a)).

For the azimuth resolution, both θ_{rin} and Ψ have certain amount of influences. If $\theta_{\text{rin}} \leq 45^\circ$, the azimuth resolution of GEO-UAV BiSAR is lower than 1.4 m (critical value of resolution). And if $\theta_{\text{rin}} > 45^\circ$, the azimuth resolution is still impacted by Ψ (see Figure 6(b)).

$$\begin{aligned} \Psi \in [0^\circ, 14^\circ] \& [44^\circ, 198^\circ] \& [230^\circ, 360^\circ] \implies D_a \leq 1.4 \text{ m}, \\ \Psi \in [15^\circ, 43^\circ] \& [199^\circ, 229^\circ] \implies D_a > 1.4 \text{ m}. \end{aligned} \quad (16)$$

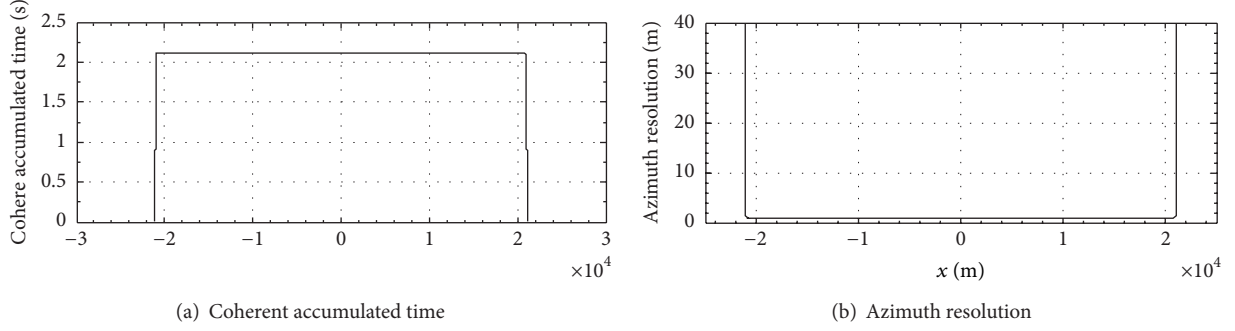
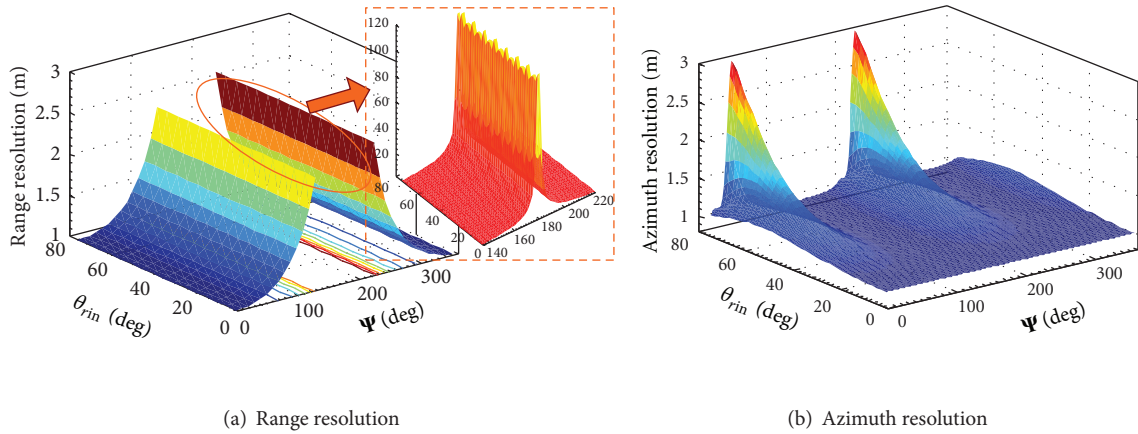
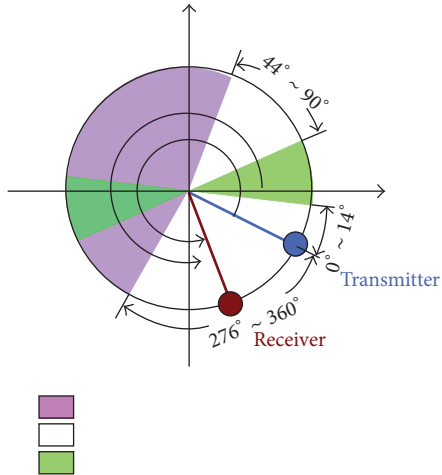
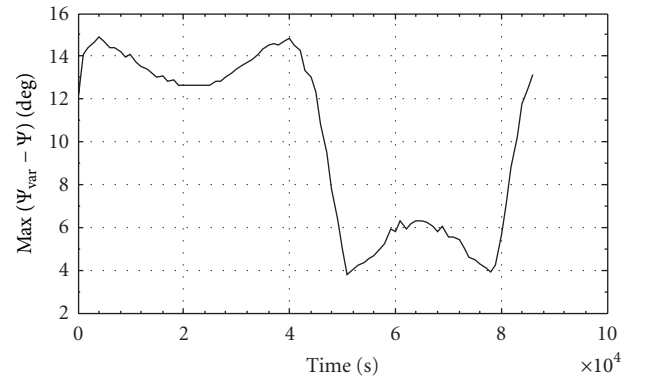
FIGURE 5: Coherent accumulated time (a) and azimuth resolution (b) ($t_0 = T_s/8$).FIGURE 6: Range resolution (a) and azimuth resolution (b) as two functions of θ_{rin} and Ψ for GEO-UAV BiSAR.

FIGURE 7: The unit location distribution of GEOSAR and UAVSAR.

To assure the high resolution of range and azimuth, the range value of Ψ is drawn in Figure 7. A unit circle represents the position projection of transmitter and receiver in xOy plane. If $\theta_{rin} \leq 45^\circ$, GEO-UAV BiSAR configuration can show high-resolution ability in the content of $\Psi \in \text{area 2 and area}$

FIGURE 8: Max($\Psi_{var} - \Psi$) in an orbital period of GEOSAR.

3, whereas we need to avoid Ψ that appears in area 1 and area 3 if $\theta_{rin} > 45^\circ$.

With the mutual movement of two platforms ($\vec{V}_{eT}(t_0 + t_a) \neq \vec{V}_R$, and $\vec{V}_{eT}(t_0 + t_a)$ is time varying), the variational range of Ψ_{var} is different in the periodical time of GEOSAR. To avoid the appearance of the dead zone2 in the clear zone, we demand to meet (10). The variational range of $\max(\Psi_{var} - \Psi)$ in the whole period of GEOSAR is shown in Figure 8. And

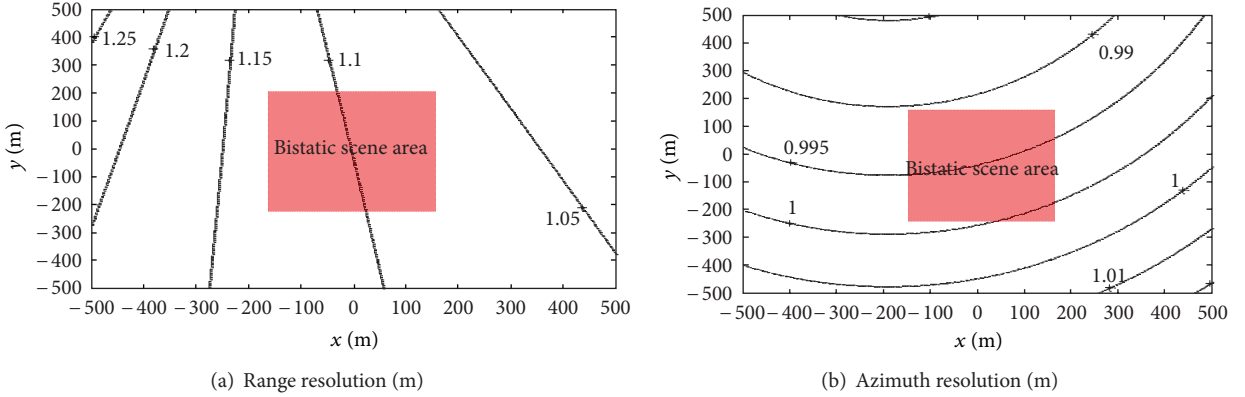


FIGURE 9: Range resolution in meters (a) and azimuth resolution in meters (b) of GEO-UAV BiSAR in xOy plane ($t_0 = T_s/8$). The red region represents the bistatic scene area.

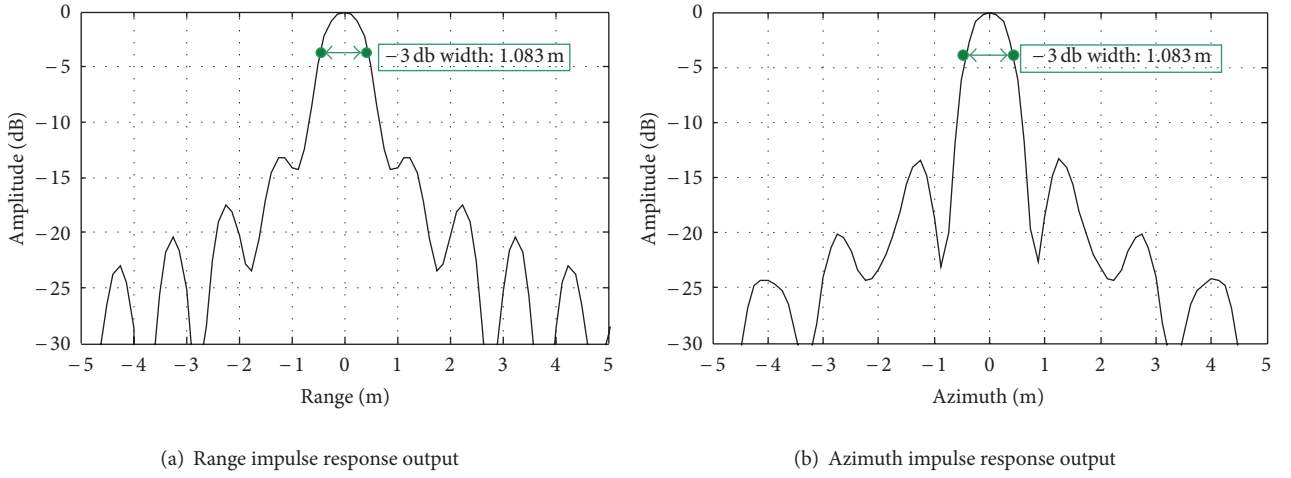


FIGURE 10: Range impulse response output (a) and azimuth impulse response output (b) for the point target ($t_0 = T_s/8$).

$\max(\Psi_{\text{var}} - \Psi)$ obtains the maximum 15° when $t_0 = T_s/20$. Hence, the proper extent of initial UAV attitude can be written as

$$\begin{aligned} \Psi &\in [0^\circ, 75^\circ] \& [291^\circ, 360^\circ] (\theta_{\text{rin}} \leq 45^\circ), \\ \Psi &\in [59^\circ, 75^\circ] \& [291^\circ, 358^\circ] (\theta_{\text{rin}} > 45^\circ). \end{aligned} \quad (17)$$

Based on the aforementioned condition, we select $\theta_{\text{rin}} = 10^\circ$ and $\Psi = 311^\circ$. Figure 9 shows the range and azimuth resolution distributions of GEO-UAV BiSAR in xOy plane ($t_0 = T_s/8$). It is worth noting that the coherent accumulated time (2.71 s in Table 3) is considered for all point target in the bistatic scene area. The bistatic scene dimensions are 400 m in range and 244 m in azimuth. And the range resolutions from 1.07 m to 1.14 m are expected along with azimuth resolutions ranging from 0.99 m to 1.00 m. These values are deduced by (8) and (9). Thus, GEO-UAV BiSAR is suitable to the image in the local area.

5.3. Frequency Domain RD Based on MSR. To evaluate the resolution of GEO-UAV BiSAR, we will focus on an image with a frequency-domain SAR processor. The corresponding

processing approach has been developed based on MSR by means of the four-level Taylor expansion [18, 19]. RD method in frequency domain is performed by four steps, that is, range compression, secondary range compression, range cell migration, and azimuth compression.

If the attitude parameters of UAVSAR are $\theta_{\text{rin}} = 10^\circ$ and $\Psi = 311^\circ$, the impulse response output at the scene center target ($t_0 = T_s/8$) is drawn in Figure 10. The corresponding measured -3 dB resolutions are 1.08 m and 1.08 m, respectively, in comparison to the theoretical values of 1.08 m and 0.99 m (in Figure 9). It can be seen that the resolution has range and azimuth broadening of about 0.3% and 9%.

6. Conclusion

Bistatic geometrical configuration using GEOSAR as a transmitter and UAVSAR as a receiver is analyzed. From a theoretical level, firstly, the variation of bistatic geometrical configuration which has influence on azimuth common coverage and coherent accumulated time is studied according to the ellipse orbital movement of GEOSAR; then, the gradient method based on GEO-UAV SAR configuration (GEOSAR

TABLE 4: Space-time analysis of GEO-UAV BiSAR.

Velocity ratio	Azimuth maximum coverage (UAVSAR position in Ox axis)	Coherent accumulated time
$k = 0$	$C_a = L_T$ ($x_R = x_R^{(0)}$)	$T_{\text{sar}} = \frac{x - x_A}{V_R}, \quad x \in [x_A, L_R + x_A],$ $T_{\text{sar}} = \frac{L_R}{V_R}, \quad x \in [L_R + x_A, L_T - L_R + x_A],$ $T_{\text{sar}} = \frac{x - L_T + L_R - x_A}{V_R}, \quad x \in [L_T - L_R + x_A, L_T + x_A].$
	$C_a = \frac{V_R L_T + V_{eT} L_R}{V_R - V_{eT}}$ $(x_R = x_R^{(0)})$	$l(x) = L_T - \frac{V_R - V_{eT}}{V_R} (x - x_A), \quad x \in \left[x_A, \frac{V_R L_T}{(V_R - V_{eT})} + x_A \right],$ $T_{\text{sar}} = \min \left(\frac{L_R}{V_R}, \frac{L_T - l(x)}{V_{eT}} \right),$
$k \in (0, 1)$	$C_a = \frac{V_R L_T + V_{eT} L_R}{V_R - V_{eT}}$ $(x_R = x_R^{(0)})$	$l(x) = \frac{V_R - V_{eT}}{V_{gT}} (x - x_A) - \frac{V_R}{V_{eT}} L_T, \quad x \in \left[\frac{V_R L_T}{(V_R - V_{gT})} + x_A, \frac{V_R L_T + V_{eT} L_R}{(V_R - V_{eT})} + x_A \right],$ $T_{\text{sar}} = \min \left(\frac{L_R}{V_R}, \frac{L_R - l(x)}{V_R} \right),$
	$C_a = \frac{V_R L_T + V_{eT} L_R}{V_{eT} - V_R}$ $(x_R = x_R^{(1)})$	$l(x) = L_R - \frac{(V_{eT} - V_R)(x - x_B)}{V_{eT}}, \quad x \in \left[x_B, \frac{V_{eT} L_R}{(V_{eT} - V_R)} + x_B \right],$ $T_{\text{sar}} = \frac{L_R - l(x)}{V_R},$
$k \in (1, +\infty)$	$C_a = \frac{V_R L_T + V_{eT} L_R}{V_{eT} - V_R}$ $(x_R = x_R^{(1)})$	$l(x) = \frac{(V_{eT} - V_R)(x - x_B)}{V_R} - L_R \frac{V_{eT}}{V_R}, \quad x \in \left[\frac{V_{eT} L_R}{(V_{eT} - V_R)} + x_B, \frac{V_R L_T + V_{eT} L_R}{(V_{eT} - V_R)} + x_B \right],$ $T_{\text{sar}} = \min \left(\frac{L_R}{V_R}, \frac{L_T - l(x)}{V_{eT}} \right),$
	$C_a = \frac{V_R L_T + V_{eT} L_R}{V_R + V_{eT}}$ $(x_R = x_R^{(1)})$	$l(x) = L_R - \frac{V_R + V_{eT}}{V_{eT}} (x - x_B), \quad x \in \left[x_B, \frac{V_{eT} L_R}{2(V_R + V_{eT})} + x_B \right],$ $T_{\text{sar}} = \min \left(\frac{L_R}{V_R}, \frac{L_R - l(x)}{V_R} \right),$
$k < 0$		$l(x) = \frac{V_R + V_{eT}}{V_R} (x - x_B) - \frac{V_{eT}}{V_R} L_R, \quad x \in \left[\frac{V_{eT} L_R}{(V_R + V_{eT})} + x_B, \frac{V_{eT} L_R + V_R L_T}{(V_{eT} + V_R)} + x_B \right],$ $T_{\text{sar}} = \min \left(\frac{L_R}{V_R}, \frac{L_T - l(x)}{V_{eT}} \right),$

exhibits the characteristics of high altitude and periodical motion) is proposed to deduce two-dimensional resolution.

Simulations illustrate that the resolution is accurately obtained from the geometrical simplification of gradient method which consists of two impact factors on the coherent accumulated time and the UAV attitude. The azimuth resolution capacity of GEO-UAV BiSAR shows a gradual decrease with coherent accumulated time reducing the relative motion of two platforms. Moreover, the proper initial selection of UAV attitude can avoid the appearance of dead zone in the swath. Such theoretical analysis, along with simulation results, further demonstrates the potential performance of GEO-UAV BiSAR that is mainly affected by the UAV attitude design when GEOSAR follows the orbital operation. Besides, the feasibility of GEO-UAV BiSAR configuration for high resolution imaging in the local field is verified.

The foregoing works in this paper inspire us to research on the existing bistatic particularities. However, the effect

of nonstationary movement related to phase center for GEOSAR and UAVSAR, which reduce the two-dimensional resolution, is ignored in this paper. In this case, the further experiments based on the nonstationary will be developed, and the resolution will be analyzed.

Appendix

See Table 4.

References

- [1] W. Edelstein, S. Madsen, A. Moussessian, and C. Chen, “Concepts and technologies for synthetic aperture radar from MEO and geosynchronous orbits,” in *Enabling Sensor and Platform Technologies for Spaceborne Remote Sensing*, Processing of SPIE, pp. 195–203, Honolulu, Hawaii, USA, November 2004.

- [2] Z. Yu, J. Chen, C. Li, Z. Li, and Y. Zhang, "Concepts, properties and imaging technologies for GEOSAR," in *MIPPR 2009: Multispectral Image Acquisition and Processing*, vol. 7494 of *Processing of SPIE*, pp. 1–7, 2009.
- [3] M. Andraschko, J. Antol, R. Baize et al., "The potential for hosted payloads at NASA," in *IEEE Aerospace Conference*, pp. 1–12, Big Sky, Mt, USA, March 2012.
- [4] C. Prati, F. Rocca, D. Giancola, and A. M. Guarnieri, "Passive geosynchronous SAR system reusing backscattered digital audio broadcasting signals," *IEEE Transactions on Geoscience and Remote Sensing*, vol. 36, no. 6, pp. 1973–1976, 1998.
- [5] "Global Earthquake Satellite System, a 20 year plan to enable earthquake prediction, 2003," NASA, JPL, May 2005, <http://www.jpl.nasa.gov/>.
- [6] D. Bruno, S. E. Hobbs, and G. Ottavianelli, "Geosynchronous synthetic aperture radar: concept design, properties and possible applications," *Acta Astronautica*, vol. 59, no. 1–5, pp. 149–156, 2006.
- [7] G. Krieger and A. Moreira, "Spaceborne bi- and multistatic SAR: potential and challenges," *IEE Proceedings: Radar, Sonar and Navigation*, vol. 153, no. 3, pp. 184–186, 2006.
- [8] J. R. Rodon, A. Broquetas, A. M. Guarnieri, and F. Rocca, "Atmospheric phase screen retrieval from GEOSAR long term acquisition," in *Proceedings of the 9th European Conference on Synthetic Aperture Radar (EUSAR '12)*, pp. 79–82, Nuremberg, Germany, April 2012.
- [9] J. Ruiz, A. Broquetas, A. Monti, and F. Rocca, "A Ku-band geosynchronous synthetic aperture radar mission analysis with medium transmitted power and medium-sized antenna," in *IEEE International Geoscience and Remote Sensing Symposium (IGARSS '11)*, pp. 2456–2459, Vancouver, Canada, July 2011.
- [10] G. L. Guttrich, W. E. Sievers, and N. M. Tomljanovich, "Wide area surveillance concepts based on geosynchronous illumination and bistatic unmanned airborne vehicles or satellite reception," in *Proceedings of the IEEE National Radar Conference*, pp. 126–131, May 1997.
- [11] J. Palmer, S. Palumbo, A. Summers, D. Merrett, and S. Howard, "DSTO's experimental geosynchronous satellite based PBR," in *International Radar Conference on Surveillance for a Safer World (RADAR '09)*, pp. 1–6, December 2009.
- [12] L. Lei, Y. Zhou, J. Li, and B. Sun, "Synchronization of GEO spaceborne-airborne bistatic SAR," in *Proceedings of IEEE International Geoscience and Remote Sensing Symposium (IGARSS '08)*, vol. 3, pp. 1209–1211, July 2008.
- [13] J. Wang, Y. Wang, R. Chen, and J. Ge, "Research on the ground resolution of bistatic forward-looking SAR with geostationary illuminator and UAV receiver," in *Proceedings of the 9th European Conference on Synthetic Aperture Radar (EUSAR '12)*, pp. 567–570, Nuremberg, Germany, April 2012.
- [14] T. Zeng, M. Cherniakov, and T. Long, "Generalized approach to resolution analysis in BSAR," *IEEE Transactions on Aerospace and Electronic Systems*, vol. 41, no. 2, pp. 461–474, 2005.
- [15] A. Moccia and A. Renga, "Spatial resolution of bistatic synthetic aperture radar: impact of acquisition geometry on imaging performance," *IEEE Transactions on Geoscience and Remote Sensing*, vol. 49, no. 10, pp. 3487–3503, 2011.
- [16] R. Wang, O. Loffeld, Y. L. Neo et al., "Focusing bistatic SAR data in airborne/stationary configuration," *IEEE Transactions on Geoscience and Remote Sensing*, vol. 48, no. 1, pp. 452–465, 2010.
- [17] R. Wang, O. Loffeld, Q. Ul-Ann, H. Nies, A. M. Ortiz, and A. Samarah, "A bistatic point target reference spectrum for general bistatic SAR processing," *IEEE Geoscience and Remote Sensing Letters*, vol. 5, no. 3, pp. 517–521, 2008.
- [18] F. H. Wong, I. G. Cumming, and Y. L. Neo, "Focusing bistatic SAR data using the nonlinear chirp scaling algorithm," *IEEE Transactions on Geoscience and Remote Sensing*, vol. 46, no. 9, pp. 2493–2505, 2008.
- [19] F. H. Wong and T. S. Yeo, "New applications of nonlinear chirp scaling in SAR data processing," *IEEE Transactions on Geoscience and Remote Sensing*, vol. 39, no. 5, pp. 946–953, 2001.
- [20] D. Bruno and S. E. Hobbs, "Radar imaging from geosynchronous orbit: temporal decorrelation aspects," *IEEE Transactions on Geoscience and Remote Sensing*, vol. 48, no. 7, pp. 2924–2929, 2010.
- [21] I. Walterscheid, T. Espeter, A. R. Brenner et al., "Bistatic SAR experiments with PAMIR and TerraSAR-X-setup, processing, and image results," *IEEE Transactions on Geoscience and Remote Sensing*, vol. 48, no. 8, pp. 3268–3279, 2010.

